AAS 23-231

A COMPARISON OF STATION-KEEPING STRATEGIES FOR HALO ORBITS

Dale A. P. Williams*, Kathleen C. Howell†, and Diane C. Davis‡

Halo orbits in the Circular Restricted Three Body Problem (CR3BP) serve as the reference motion for several current and planned missions in cislunar space. Many of these orbits are linearly unstable and, thus, require some form of an orbit maintenance strategy. Two existing orbit maintenance strategies for halo orbits are a phase-augmented x-axis crossing control approach and Floquet Mode Control scheme. A comparison of these two strategies is examined, with an emphasis on the underlying dynamics that the strategies exploit. Similar orbit maintenance maneuvers are found between the two strategies under certain conditions. A third station-keeping strategy that leverages information from the Cauchy-Green Strain Tensor is also introduced and compared with the aforementioned approaches.

INTRODUCTION

Halo orbits exist as periodic in the Circular Restricted Three Body Problem (CR3BP) and originate near the L_1 and L_2 equilibrium points. These orbits exhibit a characteristic symmetry accross the xz-plane as viewed in a rotating frame that is defined by the primary system. Near Rectilinear Halo Orbits (NRHOs) are a subset of this family of orbits that are characterized by their near stability in the linear sense.[1] Earth-Moon NRHOs are a focus of current practical interest to NASA and the broader space community. The 9:2 synodic-resonant NRHO is currently the planned reference orbit for NASA's Gateway outpost, a component of the Artemis program to return humans to the Moon sometime in the 2020s.[2] CAPSTONE, launched in 2022, is currently flying in the same NRHO as a pathfinding mission for Gateway.[3] Unstable, as well as nearly stable, halo orbits such as the 9:2 NRHO require an orbit maintenance strategy to maintain a spacecraft in the vicinity of the desired orbit. One possible strategy for xz-symmetric orbits in the CR3BP is a scheme to target a particular state component at subsequent crossings of the orbit plane of symmetry. Such a strategy was implemented for station-keeping of the ARTEMIS/THEMIS extended mission with a specific x-velocity targeted at subsequent crossings of the symmetry plane.[4,5] Gateway's planned station-keeping strategy is a modified, phase-augmented crossing control approach. This scheme places maneuvers at an osculating true anomaly value equal to 200° for effective phase control and targets a rotating x-velocity and arrival time at perilune after approximately 6.2 revolutions downstream.[6]

Floquet Mode Control (FMC) is an alternative station-keeping strategy that explicitly incorporates the linear stability information from a periodic orbit. In this approach, a maneuver is estimated that eliminates the unstable component of a six-dimensional spacecraft state, as measured in terms of an estimated variation from the reference orbit at the maneuver epoch.[7–9] Previous authors have

*Graduate Student, School of Aeronautics and Astronautics, Purdue University, West Lafayette, IN 47907; will1738@purdue.edu

†Hsu Lo Distinguished Professor, School of Aeronautics and Astronautics, Purdue University, West Lafayette, IN, 47907; howell@purdue.edu

‡Aerospace Engineer, NASA Johnson Space Center, Houston, TX, 77058; diane.c.davis@nasa.gov

identified a correlation between maneuvers constructed using a velocity-constraint crossing control approach and the position component of the stable eigenvector associated with the monodromy matrix for the reference orbit.[5,6] More recently, Farrés et al. demonstrate that the two strategies share common geometrical features by assessing variational state components in terms of time-periodic Floquet modes.[10] This investigation employs a similar strategy to assess similarities between FMC and a phase-augmented crossing control approach.

Other authors leverage dynamical information afforded by the Cauchy-Green Strain Tensor (CGT) to both station-keep halo orbits and to assess the effectiveness of other station-keeping strategies. Guzzetti et al. use the CGT to estimate an attainable region for a given maneuver magnitude and then construct a least-squares solution to determine a corresponding maneuver direction,[11] while Muraldiharan and Howell employ information from the eigendecomposition of the CGT to identify advantageous maneuver locations in Near Rectillinear Halo Orbits (NRHOs).[12] In the current investigation, an FMC-inspired CGT station-keeping strategy is also examined. This strategy, termed Principal Stretching Direction Control (PSDC), leverages the presence of stretching and restoring directions to construct a maneuver to reduce the magnitude of a spacecraft's variational state over a specified horizon time.

This investigation seeks to compare a phase augmented velocity crossing control approach, Floquet Mode Control, and PSDC within the context of the 9:2 synodic resonant NRHO. Algorithm performance, as well as to the underlying dynamics leveraged by each of the strategies, are assessed. Modifications to the conventional Floquet Mode Control algorithm are also introduced to improve orbit phase maintenance in the NRHO. The PSDC control algorithm is formulated and its effectiveness is demonstrated for the 9:2 NRHO.

THE CIRCULAR RESTRICTED THREE BODY PROBLEM

The Circular Restricted Three Body Problem (CR3BP) is the dynamical basis for this analysis (specifically, the Earth - Moon CR3BP). This model is time-autonomous and describes the motion of an object of negligible mass, P_3, under the gravitational influence of two bodies, P_1 and P_2 (denoted the primary system). In this model, it is assumed that the two primaries follow circular orbits about their common barycenter (B) and that P_1 is the primary of larger mass.

To formulate the nondimensional CR3BP equations of motion in their conventional form, characteristic quantities (that is length l^*, time t^*, and mass m^*) are defined. The characteristic length is selected as the distance between the primaries (often measured in km), and the characteristic time is defined as the reciprocal of the system mean motion (often measured in seconds). Finally, the total mass of the primary system defines the characteristic mass, m^*. This definition for m^* allows for the convenient characterization of a system in terms of a single mass parameter, $\mu = m_2/m^*$, where m_2 is the mass of P_2. With this definition of μ, the non-dimensional distance between P_1 and the barycenter B is denoted μ and the non-dimensional distance between P_2 and B is labeled $1-\mu$.

The non-dimensional equations of motion for P_3 with respect to the system barycenter are formulated in a rotating frame defined by P_1 and P_2. This rotating frame is denoted by the $\hat{x}$, $\hat{y}$, and $\hat{z}$ directions as illustrated in Figure 1. The coordinate directions $\hat{X}$, $\hat{Y}$, and $\hat{Z}$ define an inertial frame with which the rotating frame is aligned at some initial time. Observe that the plane of primary motion defines the $\hat{x}$-$\hat{y}$ plane. Within the rotating frame, the position of P_3 with respect to the barycenter is expressed as $\boldsymbol{\rho} = x\hat{x} + y\hat{y} + z\hat{z}$. Throughout, boldface quantities denote vectors. The

non-dimensional distances between P_3 and P_1 and P_3 and P_2 are defined as d and r, respectively, and expressed as

$$d = \sqrt{(x+\mu)^2 + y^2 + z^2} \tag{1}$$

$$r = \sqrt{(x-1+\mu)^2 + y^2 + z^2}. \tag{2}$$

The equations of motion for P_3 with respect to the system barycenter are given in this rotating frame by

$$\ddot{x} = 2\dot{y} + \frac{\partial U^*}{\partial x}, \qquad \ddot{y} = -2\dot{x} + \frac{\partial U^*}{\partial y}, \qquad \ddot{z} = \frac{\partial U^*}{\partial z}. \tag{3}$$

In these equations, U^* is a pseudo-potential function defined by

$$U^* = \frac{(1-\mu)}{d} + \frac{\mu}{r} + \frac{1}{2}\left(x^2 + y^2\right). \tag{4}$$

Note that U^* is only a function of the position of P_3 in the rotating frame and the mass parameter, μ. The CR3BP equations admit one integral of the motion, i.e. the Jacobi Constant, that can be expressed as

$$\mathcal{J} = 2U^* - (\dot{x}^2 + \dot{y}^2 + \dot{z}^2). \tag{5}$$

Of relevance to this investigation, this first integral of the motion ensures that periodic orbits in the CR3BP exist in families.[13]

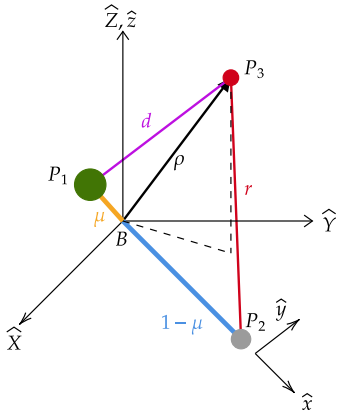

Figure 1: CR3BP Rotating Frame within Inertial Frame

LINEAR VARIATIONAL EQUATIONS

Given the non-dimensional equations of motion, a focus for any station-keeping application is the variational state of a spacecraft (P_3) with respect to some reference periodic orbit. Define $\delta\boldsymbol{x}$ as the six-dimensional (position and velocity) state vector for non-dimensional variations, measured with respect to some reference trajectory, $\boldsymbol{x}^*(t)$. The state transition matrix (STM) associated with this reference orbit or trajectory arc relates variations over time. Specifically, the STM maps an initial (non-dimensional) variation from a reference to a variation at some subsequent time, i.e.,

$$\delta\boldsymbol{x}(t_f) = \Phi(t_f, t_0)\delta\boldsymbol{x}(t_0). \tag{6}$$

Knowledge about the evolution of variations with respect to a reference orbit is essential for the design of effective station-keeping strategies.

While the state transition matrix relates variations under a linearized flow, the Cauchy Green Strain Tensor, $\mathcal{C}$, describes the expansion and contraction of the variational phase space. Specifically, the CGT describes the evolution of $\|\delta\boldsymbol{x}\|$ under the flow, such that

$$\|\delta\boldsymbol{x}(t)\|^2 = \delta\boldsymbol{x}^T(t_0)\Phi^T(t,t_0)\Phi(t,t_0)\delta\boldsymbol{x}(t_0) = \delta\boldsymbol{x}^T(t_0)\mathcal{C}(t,t_0)\delta\boldsymbol{x}(t_0), \tag{7}$$

where superscript T denotes the transpose of a matrix. The eigenvalues and eigenvectors corresponding to the CGT (or, similarly, the singular values and vectors of the STM) provide useful information concerning the local stretching and contraction of the phase space, leveraged by previous authors for station-keeping applications.[11,12,14]

FLOQUET THEORY

When a reference trajectory is periodic (i.e., $\boldsymbol{x}^*(t+\tau) = \boldsymbol{x}^*(t)$), Floquet theory offers a useful decomposition of the STM. Specifically,

$$\Phi(t,t_0) = E(t)e^{B(t-t_0)}E^{-1}(t_0), \tag{8}$$

where $E(t+\tau) = E(t)$ and B is a Jordan form matrix containing the Poincaré exponents, η_i, associated with the reference periodic orbit (and that may be complex). Since $E(t)$ is τ-periodic, it is clear from Equation (8) that

$$\Phi(t_0+\tau,t_0) = E(t_0)e^{B\tau}E^{-1}(t_0), \tag{9}$$

$$= E(t_0)\Lambda E^{-1}(t_0), \tag{10}$$

where

$$E(t_0) = \begin{bmatrix}\boldsymbol{e}_1(t_0) & \boldsymbol{e}_2(t_0) & \cdots & \boldsymbol{e}_6(t_0)\end{bmatrix}. \tag{11}$$

Equation (9) defines an eigenvalue problem for the monodromy matrix associated with the underlying periodic orbit. The eigenvalues, λ_i, of any periodic orbit in the CR3BP (also called characteristic multipliers) always occur in reciprocal pairs. Furthermore, a pair of these characteristic multipliers are located at unity.[1] Throughout this investigation, it is assumed that a reference periodic orbit has only one mode of instability and one mode of stability. This assumption is consistent with the stability properties of the 9:2 synodic resonant NRHO. The symplectic structure of the CR3BP equations of motion then implies the existence of characteristic multipliers $|\lambda_1| > 1$, $|\lambda_2| = 1/|\lambda_1|$, $\lambda_3 = \bar{\lambda}_4$ (complex conjugates of unit magnitude), and $\lambda_5 = \lambda_6 = 1$. Note that the reciprocal pairing of the characteristic multipliers ensures that λ_1 and λ_2 are real numbers. The Poincaré exponents are related to the characteristic multipliers of the monodromy matrix, i.e.,

$$\eta_i = \frac{1}{\tau}\ln(\lambda_i). \tag{12}$$

The reciprocal pairing of the characterisitic multipliers also implies that the Poincaré exponents occur in positive/negative pairs. Furthermore, since λ_3 is assumed to be complex and of unit magnitude, the Poincaré exponent η_3 is purely imaginary. That is $\eta_3 = j\Gamma$, where $j = \sqrt{-1}$. The Poincaré exponents provide useful information about the modes of stability and instability associated with a periodic orbit.

Of special note to this investigation are the two characteristic multipliers at unity, often termed the trivial pair. The first of these eigenvalues arises from the fact that the CR3BP is time-autonomous and corresponds to a shift in phase (or, equivalently, initial time) along the periodic orbit. A second unity eigenvalue is guaranteed because the CR3BP possesses a constant first integral of the motion. This second eigenvalue indicates the existence of other nearby periodic orbits at different values of the Jacobi Constant. Notably, the unity eigenvalue only possesses a geometric multiplicity of one and is thus defective. Hence, a generalized eigenvector must be constructed to solve the generalized eigenvalue problem in Equation (9).

The presence of a generalized eigenvector associated with the monodromy matrix corresponding to a periodic orbit in the CR3BP is related to the change in orbit period with respect to Jacobi Constant, as noted by Simó et al.[7] Let $\boldsymbol{x}_p$ denote a specific initial condition on a periodic orbit. Following Wiesel and Pohlen,[13] it is possible to express this initial condition as a member of a two-parameter family such that

$$\boldsymbol{x}_p = \boldsymbol{x}_p(\mathcal{J}, \phi = \omega(\mathcal{J})(t - t_0)), \tag{13}$$

where ϕ represents a phase angle and ω is defined as the frequency for the orbit (and is a function of the Jacobi Constant). Since the model is time-autonomous and conservative, two independent perturbations that yield other nearby periodic solutions, $\delta\boldsymbol{x}_t$ and $\delta\boldsymbol{x}_{\mathcal{J}}$, are defined. More explicitly,

$$\delta\boldsymbol{x}_{t_0} = \frac{\partial \boldsymbol{x}_p}{\partial \phi}\frac{\partial \phi}{\partial(-t_0)}\delta(-t_0) = \omega(\mathcal{J})\frac{\partial \boldsymbol{x}_p}{\partial \phi}\delta(-t_0) = \frac{d\boldsymbol{x}_p}{dt}\delta t \tag{14}$$

$$\delta\boldsymbol{x}_{\mathcal{J}} = \frac{\partial \boldsymbol{x}_p}{\partial \mathcal{J}}\delta\mathcal{J} + \frac{\partial \boldsymbol{x}_p}{\partial \phi}\frac{d\omega}{d\mathcal{J}}(t - t_0)\delta\mathcal{J} = \frac{\partial \boldsymbol{x}_p}{\partial \mathcal{J}}\delta\mathcal{J} + \frac{1}{\omega}\frac{d\boldsymbol{x}_p}{dt}\frac{d\omega}{d\mathcal{J}}(t - t_0)\delta\mathcal{J}. \tag{15}$$

Perturbations in the directions defined by Equations (14) and (15) imply

$$\Phi(t_0 + \tau, t_0)\begin{bmatrix} \frac{d\boldsymbol{x}_p}{dt} & \frac{\partial \boldsymbol{x}_p}{\partial \mathcal{J}} \end{bmatrix} = \begin{bmatrix} \frac{d\boldsymbol{x}_p}{dt} & \frac{\partial \boldsymbol{x}_p}{\partial \mathcal{J}} \end{bmatrix}\begin{bmatrix} 1 & \frac{1}{\omega}\frac{d\omega}{d\mathcal{J}}\tau \\ 0 & 1 \end{bmatrix}. \tag{16}$$

The solution of this generalized eigenvalue problem permits the accurate computation of the columns of $E(t_0)$ corresponding to the trivial pair.

Once the eigenvectors associated with the trivial pair have been computed, it is easy to determine the form of the exponential matrix $e^{B\tau}$ in Equation (9). Specifically, this matrix can be expressed as

$$e^{B\tau} = \begin{bmatrix} \lambda_1 & 0 & 0 & 0 & 0 & 0 \\ 0 & \frac{1}{\lambda_1} & 0 & 0 & 0 & 0 \\ 0 & 0 & \lambda_3 & 0 & 0 & 0 \\ 0 & 0 & 0 & \bar{\lambda}_3 & 0 & 0 \\ 0 & 0 & 0 & 0 & 1 & \frac{1}{\omega}\frac{d\omega}{d\mathcal{J}}\tau \\ 0 & 0 & 0 & 0 & 0 & 1 \end{bmatrix}. \tag{17}$$

Note that the matrix $e^{B\tau}$ has complex entries corresponding to λ_3. From the matrix logarithm, it is apparent that

$$B = \begin{bmatrix} \eta_1 & 0 & 0 & 0 & 0 & 0 \\ 0 & -\eta_1 & 0 & 0 & 0 & 0 \\ 0 & 0 & \eta_3 = i\Gamma & 0 & 0 & 0 \\ 0 & 0 & 0 & \eta_4 = -i\Gamma & 0 & 0 \\ 0 & 0 & 0 & 0 & 1 & \varepsilon = \frac{1}{\omega}\frac{d\omega}{d\mathcal{J}} \\ 0 & 0 & 0 & 0 & 0 & 1 \end{bmatrix}. \tag{18}$$

Given Equation (8), it is then possible to write

$$\Phi(t,t_0)\boldsymbol{e}_1(t_0) = \boldsymbol{e}_1(t)e^{\eta_1 t} \tag{19}$$

$$\Phi(t,t_0)\boldsymbol{e}_2(t_0) = \boldsymbol{e}_2(t)e^{-\eta_1 t}. \tag{20}$$

By assumption, $\eta_1 > 0$, implying that Equation (19) defines a mode of exponential growth (instability) associated with a periodic orbit, while Equation (20) is associated with a mode of stability. Similarly, the equations

$$\Phi(t,t_0)\boldsymbol{e}_5(t_0) = \boldsymbol{e}_5(t) \tag{21}$$

$$\Phi(t,t_0)\boldsymbol{e}_6(t_0) = \varepsilon\boldsymbol{e}_5(t)(t-t_0) + \boldsymbol{e}_6(t). \tag{22}$$

define the evolution of the perturbations associated with the trivial pair. Of particular note is the linear growth term associated with Equation (22). Similar equations are also derived for $\boldsymbol{e}_3(t)$ and $\boldsymbol{e}_4(t)$, but are complex valued. It is advantageous to note that $\boldsymbol{e}_3(t_0) = \bar{\boldsymbol{e}}_4(t_0)$ and thus $\boldsymbol{e}_3(t) = \bar{\boldsymbol{e}}_4(t)$ from Equation (8). Defining $\boldsymbol{f}_3(t) = (\boldsymbol{e}_3(t) + \boldsymbol{e}_4(t))/2$ and $\boldsymbol{f}_4(t) = (\boldsymbol{e}_3(t) - \boldsymbol{e}_4(t)/2j$, it can be demonstrated[10] that

$$\Phi(t,t_0)\boldsymbol{f}_3(t_0) = \boldsymbol{f}_3(t)\cos(\Gamma t) - \boldsymbol{f}_4(t)\sin(\Gamma t) \tag{23}$$

$$\Phi(t,t_0)\boldsymbol{f}_4(t_0) = \boldsymbol{f}_3(t)\sin(\Gamma t) + \boldsymbol{f}_4(t)\cos(\Gamma t), \tag{24}$$

where $\boldsymbol{f}_3$ and $\boldsymbol{f}_4$ are real vectors. Defining $\boldsymbol{f}_1(t_0) = \boldsymbol{e}_1(t_0)$, $\boldsymbol{f}_2(t_0) = \boldsymbol{e}_2(t_0)$, $\boldsymbol{f}_5(t_0) = \boldsymbol{e}_5(t_0)$, and $\boldsymbol{f}_6(t_0) = \boldsymbol{e}_6(t_0)$ (all of which are real valued), the Equation (8) is rewritten as

$$\Phi(t,t_0) = F(t)e^{J(t-t_0)}F^{-1}(t_0), \tag{25}$$

where

$$F(t) = \begin{bmatrix}\boldsymbol{f}_1(t) & \boldsymbol{f}_2(t) & \cdots & \boldsymbol{f}_6(t)\end{bmatrix}, \tag{26}$$

$$e^{J(t-t_0)} = \begin{bmatrix} e^{\eta_1(t-t_0)} & 0 & 0 & 0 & 0 & 0 \\ 0 & e^{-\eta_1(t-t_0)} & 0 & 0 & 0 & 0 \\ 0 & 0 & \cos(\Gamma(t-t_0)) & \sin(\Gamma(t-t_0)) & 0 & 0 \\ 0 & 0 & -\sin(\Gamma(t-t_0)) & \cos(\Gamma(t-t_0)) & 0 & 0 \\ 0 & 0 & 0 & 0 & 1 & \varepsilon(t-t_0) \\ 0 & 0 & 0 & 0 & 0 & 1 \end{bmatrix}. \tag{27}$$

The expression for the STM in Equation (25) is convenient as it ensures that $F(t_0)$ is always a real matrix.

A formulation for the variations relative to a periodic orbit in terms of the basis described in Equation (26) is useful because it partitions the variational space into subspaces that are invariant in the linear sense. Specifically, Equation (6) coupled with Equation (25) allows the variational state $\delta\boldsymbol{x}(t)$ to be expressed as

$$\delta\boldsymbol{x}(t) = F(t)e^{J(t-t_0)}\boldsymbol{\alpha} \tag{28}$$

where $\boldsymbol{\alpha}$ is a constant vector of real values that are constructed from

$$\boldsymbol{\alpha} = \begin{pmatrix}\alpha_1 & \alpha_2 & \cdots & \alpha_6\end{pmatrix}^T = F^{-1}(t_0)\delta\boldsymbol{x}(t_0). \tag{29}$$

The components of $\boldsymbol{\alpha}$ provide immediate information about the evolution of the variations near a reference periodic orbit. For example, a variational state with $\alpha_1 \neq 0$ exhibits exponential growth over time if uncorrected by some orbit maintenance strategy.

STATION-KEEPING STRATEGIES

In this investigation, three station-keeping strategies are examined with the goal of exploring the underlying dynamics that each strategy exploits and any similarities that exist in the results from these approaches. Throughout, the reference periodic orbit is the CR3BP 9:2 synodic resonant NRHO with an orbital period of approximately 6.56 days. For all three of the station-keeping strategies considered, maneuvers are placed at an osculating true anomaly of 200° to be consistent with the planned orbit maintenance strategy for Gateway, as outlined by Davis et. al.[6]

Phase Augmented Crossing Control (PACCMAN)

Recall that the planned orbit maintenance strategy for Gateway is a modified, phase-augmented, x-axis crossing control strategy (abbreviated to PACCMAN for **P**hase **A**ugmented **C**rossing **C**ontrol **MAN**euvers). In the PACCMAN scheme, a maneuver is computed at an osculating true anomaly equal to 200° that seeks to achieve a specific rotating x-velocity and arrival time at perilune approximately 6.2 revolutions downstream, as detailed by Davis et al.[6] In the CR3BP, this strategy is analogous to achieving

$$\dot{x} = 0 \pm v_{tol}$$
$$t_p = t_{targ} \pm t_{tol}$$

at perilune after approximately 6.2 revs. The target time, t_{targ}, is constructed from

$$t_{targ} = C_t(t_{p,ref} - t_p) + t_p. \tag{30}$$

where $t_{p,ref}$ is the arrival time at perilune on the nominal orbit (no errors) and C_t is a selected scalar weighting quantity. Optionally, computed maneuvers that are smaller than some threshold, ΔV_{min} are waived to produce lower station-keeping maneuver costs. In this investigation, parameters are chosen to be consistent with those specified for Gateway[6] and tabulated in Table 1. Note that these parameters significantly affect results and are chosen according to mission priorities.

Table 1: PACCMAN Parameters

Maneuver TA	v_{tol}	t_{tol}	C_t	ΔV_{min}
200°	0.45 m/s	15 min	0.3	3 cm/s

For Gateway's planned station-keeping procedure, maneuvers are first determined that satisfy the constraint on $\dot{x}$ using a Newton-Raphson iteration scheme. Forward differencing aids in producing the necessary gradients. The computed maneuver from targeting $\dot{x}$ only is then used as an initial guess for targeting both $\dot{x}$ and t_p, as outlined by Davis et al.[6] The PACCMAN targeting problem is, notably, under-constrained and evaluated with a minimum norm solution that minimizes the size of the maneuver update within each iteration. To produce smaller maneuver magnitudes that enhance the stability of the algorithm and offer lower station-keeping maneuver costs, an attenuated update is also applied in the Newton-Raphson scheme when targeting both $\dot{x}$ and t_p. Specifically, updates with magnitudes larger than 3 cm/s are limited to be exactly 3 cm/s in the appropriate direction during the update.

Floquet Mode Control (FMC)

Floquet Mode Control (FMC) explicitly incorporates stability information from Floquet theory to estimate a maneuver that eliminates the unstable component of a spacecraft variational state with respect to a periodic orbit. From Equation (28), the variational state of a spacecraft with respect to a periodic orbit is expressed as a linear combination of time-periodic Floquet modes[7–9] such that

$$\delta \boldsymbol{x}(t) = \sum_{i=1}^{6} \alpha_i \boldsymbol{f}_i(t). \tag{31}$$

Recall that $\boldsymbol{f}_1(t)$ is associated with a single unstable mode for the periodic orbit. Floquet Mode Control traditionally constructs an impulsive maneuver ($\Delta \boldsymbol{V}$) to remove any unstable component of the variational state,[7,8,10,15] i.e.,

$$\delta \boldsymbol{x}(t_0) + \begin{bmatrix} 0 \\ \Delta \boldsymbol{V} \end{bmatrix} = \sum_{i=2}^{6} \alpha_i \boldsymbol{f}_i(t_0). \tag{32}$$

Here, t_0 represents the time of the current station-keeping maneuver. The vectors $\boldsymbol{f}_i(t_0)$ are then evaluated from a monodromy matrix associated with a specific state on the reference periodic orbit. This state is either the isochronous state on the reference periodic orbit at the current maneuver epoch or a correspondence to a specific reference location on the periodic orbit (for example, an osculating true anomaly) . In this investigation, the reference monodromy matrix is assessed based on a correspondence in the maneuver true anomaly, unless otherwise indicated.

The Floquet Mode Control problem is under-constrained and a solution using a minimum norm criterion is certainly an option. However, a conventional minimum norm solution incorporates the coefficients, α_{2-6}, as well as the $\Delta \boldsymbol{V}$ vector. Notably, a minimum norm solution to Equation (32) does not minimize the magnitude of the $\Delta \boldsymbol{V}$. Farrés et al. note that solving Equation (32) with an additional constraint on minimizing $\|\Delta \boldsymbol{V}\|$ or constraining the direction of the maneuver can produce similar results to a velocity-constraint crossing control strategy.[10] In this investigation, a more general formulation of the FMC problem is examined for greater flexibility in applications. Define the matrix

$$\mathcal{F} = \begin{bmatrix} \boldsymbol{f}_1^{pos}(t_0) & \boldsymbol{f}_2^{pos}(t_0) & \cdots & \boldsymbol{f}_6^{pos}(t_0) & 0_{3\times 3} \\ \boldsymbol{f}_1^{vel}(t_0) & \boldsymbol{f}_2^{vel}(t_0) & \cdots & \boldsymbol{f}_6^{vel}(t_0) & -I_{3\times 3} \end{bmatrix} \tag{33}$$

and the control vector

$$\boldsymbol{\alpha}^* = \begin{bmatrix} \boldsymbol{\alpha} \\ \Delta \boldsymbol{V} \end{bmatrix}. \tag{34}$$

Select a diagonal weighting matrix W_{flo} and the reference vector $\boldsymbol{b}$. Then, from Equation (31) the FMC problem is reformulated as the solution to the equation

$$\delta \boldsymbol{x}(t_0) = \mathcal{F} \boldsymbol{\alpha}^*, \tag{35}$$

that minimizes an objective function

$$J_{flo} = \frac{1}{2} \|W_{flo}(\boldsymbol{\alpha}^* - \boldsymbol{b})\|^2. \tag{36}$$

Selecting a weighting matrix and reference vector that severely penalizes a large state component associated with a given direction functionally removes that component from the spacecraft variational

state. Such an approach delivers the FMC objective when a large weight is selected to penalize a state component along the unstable direction. One advantage of the formulation in Equations (35) and (36), however, is that control is then easily enacted over other Floquet modes as well and straightforwardly weighted against maneuver magnitude.

Principal Stretching Direction Control (PSDC)

One disadvantage of Floquet Mode Control is the requirement to construct the necessary Floquet mode vectors. Evaluating these modes in the CR3BP is straightforward, but not practical in applications where precisely periodic solutions no longer exist (for example, an ephemeris force model). Gomez et al. note that in higher fidelity models, these modes are often estimated by using solutions from the CR3BP.[9] Another alternative, however, is leveraging information from the Cauchy Green Strain Tensor (CGT) to construct a dynamically informed station-keeping strategy that does not require a periodic reference solution. Previous authors have exploited information from the CGT to both accomplish the station-keeping task and to assess the effectiveness of other station-keeping strategies. Guzzetti et al. used the CGT to estimate an attainable region for a given maneuver magnitude and then constructed a least-squares solution to determine a maneuver direction,[11] while Muraldiharan and Howell used information from the eigendecomposition of the CGT to identify advantageous maneuver locations in Near Rectillinear Halo Orbits (NRHOs).[12] In this investigation, a FMC inspired station-keeping strategy that leverages information from the CGT is examined.

The CGT provides a linear approximation for the growth in total magnitude (position and velocity) of a variational state over time (Equation (7)). Specifically, the eigenvalues $\varsigma_1^2 \geq \varsigma_2^2 \geq \cdots \geq \varsigma_6^2$ from the CGT and the associated six-dimensional unit eigenvectors, $\boldsymbol{\xi}_i$, represent the directions of expansion and contraction in the linear variational phase space. Defining $\boldsymbol{u}_i = (\Phi(t,t_0)\boldsymbol{\xi}_i)/\|\Phi(t,t_0)\boldsymbol{\xi}_i\|$, it is apparent that

$$\boldsymbol{u}_i\varsigma_i = \Phi(t,t_0)\boldsymbol{\xi}_i, \tag{37}$$

representing the singular value decomposition (SVD) of the state transition matrix. Notably, variations in the directions $\boldsymbol{\xi}_i$ corresponding to $\varsigma_i > 1$ see a growth in magnitude over the specified time interval and are often termed stretching directions, whereas variations in directions corresponding to $0 < \varsigma_i < 1$ decrease in magnitude and are termed restoring directions.[12] An example of the mapping defined by Equation (37) is illustrated for a two-dimensional phase space in Figure 2.

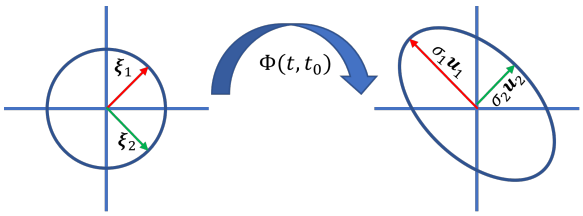

Figure 2: Principal Direction Example

In this investigation, a station-keeping strategy that eliminates the components of a spacecraft variational state corresponding to stretching directions is formulated. For a given time horizon, t_{horiz} and a state transition matrix, $\Phi(t_0+t_{horiz},t_0)$ corresponding to isochronous variatons relative

to a reference trajectory, the variational state at some maneuver time t_0 can be represented as a linear combination of the orthonormal CGT eigenvector directions, i.e.,

$$\delta \boldsymbol{x}(t_0) = \sum_{\substack{i \\ \varsigma_i > 1}} \beta_i \boldsymbol{\xi}_i + \sum_{\substack{i \\ 0 < \varsigma_i \leq 1}} \beta_i \boldsymbol{\xi}_i. \tag{38}$$

For three or fewer stretching directions, it is possible to produce a maneuver such that

$$\delta \boldsymbol{x}(t_0) + \begin{bmatrix} 0 \\ \Delta \boldsymbol{V} \end{bmatrix} = \sum_{\substack{i \\ 0 < \varsigma_i \leq 1}} \beta_i \boldsymbol{\xi}_i, \tag{39}$$

ensuring that the spacecraft exists in the restoring subspace over the specified horizon time and, thus, the magnitude of the variational state vector will descreases after t_{horiz}. This strategy is termed Principal Stretching Direction Control (PSDC) and is similar to Floquet Mode Control except that the directions representing the spacecraft variational state are the orthogonal CGT eigenvector directions instead of the Floquet mode vectors of the orbit. Similar to FMC, a weighted minimum norm is available when Equation (39) is underdetermined. For the 9:2 synodic resonant NRHO and a reference state corresponding to an osculating true anomaly of 200°, the state transition matrix possesses three stretching and three restoring directions for arbitrary time horizons up to twenty revolutions of the orbit, as illustrated in the singular value plot in Figure 3. Hence, for the station-keeping application in this investigation, Equation (39) defines a square system and a unique maneuver is determined for any of the time horizons that appear in the plot.

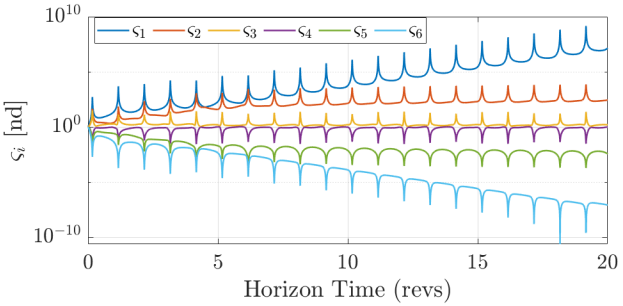

Figure 3: STM Singular Values for 9:2 NRHO at TA = 200°

PACCMAN RESULTS

Orbit maintenance maneuver (OMM) patterns are first explored for the PACCMAN station-keeping strategy in the 9:2 synodic resonant NRHO. Station-keeping operations are modeled in a Monte Carlo simulation with 100 trials, each for 840 revolutions of the NRHO (or approximately 15 years). One OMM opportunity is allowed per revolution of the orbit and is executed at an osculating true anomaly value of 200°. An OMM is waived if the magnitude of the constructed maneuver is smaller than 3 cm/s. Modeled errors in each of the Monte Carlo trials include orbit insertion error, navigation errors, momentum wheel desaturation errors, and maneuver execution errors. Insertion and navigation errors are modeled by sampling a mean-zero Gaussian distribution for each state component with 3σ values specified in Table 2. Momentum wheel desaturation errors are implemented as a maneuver in a randomly sampled direction with a 3σ magnitude of 1 cm/s. Maneuver

execution errors are modeled in terms of a pointing direction error, fixed magnitude error, and percent error calculated from the magnitude of the constructed maneuver. Magnitude and direction errors are both sampled from mean zero Gaussian distributions with 3σ values specified in Table 2. The selected values in this investigation are consistent with those considered by Davis et. al.[6]

Table 2: Error Modeling

Category	Error Type	3σ Value	Location
Desaturation Error	Random $\Delta \boldsymbol{V}$	1 cm/s	Osculating true anomalies of 330°, 0.1°, 30°, and 160°
Navigation Error	Position Velocity	1.5 km 0.8 cm/s	24 hours prior to OMM
Insertion Error	Position Velocity	2 km 2 cm/s	First apolune only
Maneuver Execution Error	Direction Fixed Magnitude Relative magnitude	1° 1.42 mm/s 1.5%	Osculating true anomaly of 200°

Station-keeping performance is assessed in terms of perilune position error, error in perilune arrival time, and cumulative station-keeping maneuver costs over the specified simulation duration. Results appear in Figure 4. From Figure 4(a) and 4(b), it can be seen that the PACCMAN strategy maintains a spacecraft within approximately 175 km and 1 hour of the reference orbit at perilune for the duration of the simulation. While some secular growth in position error can be seen in Figure 4(a), Davis et. al note that such error can be eliminated through the introduction of damping maneuvers.[6] The cumulative ΔV for all trials remains below 25 m/s (Figure 4(c)). In Figure 4(d), all maneuvers are observed to fall in a well-defined plane. This identified maneuver plane corresponds with that found in Davis et al.[6] The parallel "stripes" of maneuvers observed in Figure 4(d) are an artifact of the attenuated update implemented in the PACCMAN strategy.

For added intuition and to clarify the underlying dynamics leveraged by the PACCMAN strategy, it is useful to focus on the components of the spacecraft state expressed in terms of a basis defined by the Floquet modes, as described by Equation (29). This analysis is similar to that introduced by Farrés et al.[10] By comparing the components of $\boldsymbol{\alpha}$ pre- and post-maneuver, the Floquet modes that the PACCMAN strategy attempts to excite and eliminate are made clear. Floquet mode vectors, $\boldsymbol{f}_i(t_0)$, are constructed from a state corresponding to a true anomaly of 200° along the reference NRHO. Of particular interest are components of the spacecraft variational state that are associated with growth or decay. Specifically, recall that α_1 is the component of a spacecraft state associated with the unstable direction, whereas α_2 is associated with the stable direction. The distributions of each of these coefficients (pre- and post-maneuver) are illustrated in Figure 5. In Figure 5(a), the post maneuver distribution for α_1 coefficients is contracted as compared to the pre-maneuver distribution. Note that the total count of maneuvers in the pre-maneuver and post-maneuver distributions is always the same; the observed contraction only implies that more post-maneuver α_1 values are close to zero. Conversely, the distribution of α_2 plotted in Figure 5(b) is seen to widen after maneuvers are executed, suggesting that the PACCMAN functionally shifts a spacecraft from the unstable subspace of the periodic orbit toward the stable subspace. Similar results are demonstrated by Farrés et al. for other halo orbits using a velocity constraint crossing control strategy.[10]

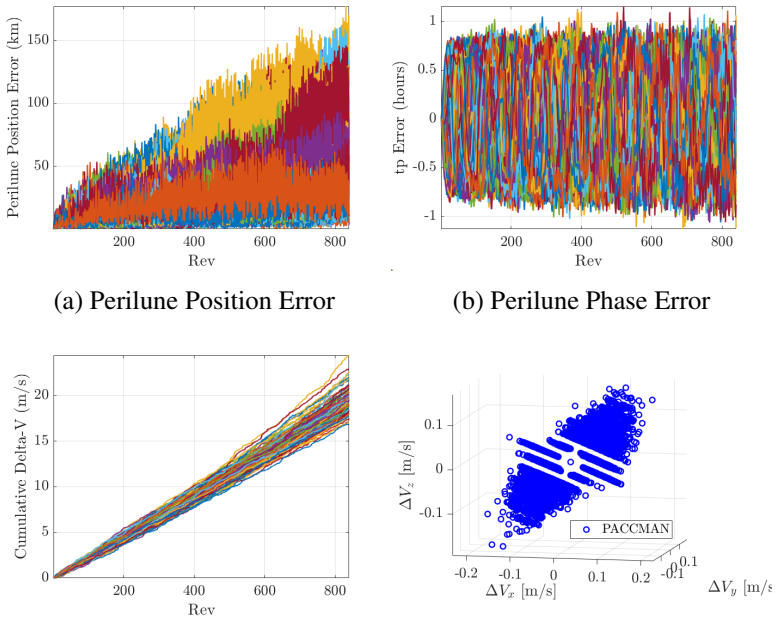

(a) Perilune Position Error (b) Perilune Phase Error

(c) Cumulative ΔV (d) Implemented Maneuvers

Figure 4: PACCMAN Monte Carlo Results Colored According to Trial Index

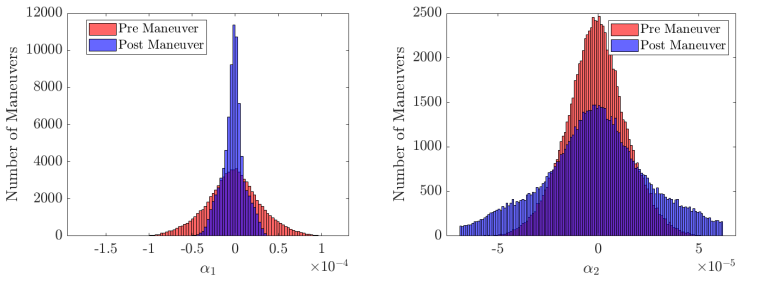

(a) Unstable Component (α_1) (b) Stable Component (α_2)

Figure 5: PACCMAN Exponential Floquet Components

The component of a variational state corresponding to $\boldsymbol{f}_6(t_0) = \boldsymbol{e}_6(t_0)$ is also of interest. From Equation (22), it can be seen that a variatonal state with a nonzero component (α_6) along the $\boldsymbol{f}_6(t_0)$ direction will experience linear growth over time. Specifically, for an initial variational state $\delta\boldsymbol{x}(t_0) = \alpha_6 \boldsymbol{f}_6(t_0)$, Equation (22) implies that

$$\delta\boldsymbol{x}(t_0 + \tau) - \delta\boldsymbol{x}(t_0) = \alpha_6 \varepsilon \tau \boldsymbol{f}_5(t_0). \tag{40}$$

Recall that $\boldsymbol{f}_5(t_0)$ corresponds to a direction along the orbit in the 6-dimensional phase space. Hence, variational states with nonzero components in the $\boldsymbol{f}_6(t_0)$ direction result in a linear drift in phase, either ahead or behind in the orbit in terms of time, after one orbit period. From Figure 6, another effect of the PACCMAN strategy is a small contraction in the α_6 distribution after OMM's are executed. This contraction suggests that another effect of the PACCMAN strategy is to reduce

the component of a spacecraft variational state along a direction associated with linear growth, at least as a result of some of the executed maneuvers.

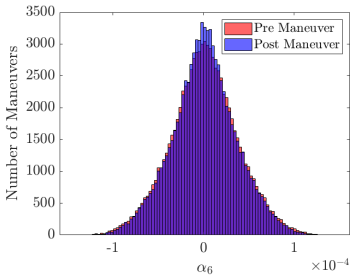

Figure 6: PACCMAN α_6 Distributions

FLOQUET MODE CONTROL RESULTS

The reduction in the variational state component α_1 associated with instability in Figure 5(a) suggests that the PACCMAN strategy may be functionally similar to Floquet Mode Control. Two forms of Floquet Mode Control are considered. The first method, that is Standard FMC, produces a maneuver that eliminates only the unstable component of a spacecraft variational state, while minimizing the size of the implemented maneuver. The second strategy, termed Modified FMC, attempts to control both the unstable component of the spacecraft variational state and the component corresponding to the direction of linear growth ($\boldsymbol{f}_6(t_0)$). The Modified FMC problem is also underdetermined and solved with a minimum ΔV approach. In both approaches, the Floquet modes used in the computation of each maneuver are extracted from a monodromy matrix associated with the reference NRHO at a true anomaly value of 200°. It is emphasized that this location does *not* imply an isochronous correspondence with the reference orbit at the epoch of each maneuver. Consistent with the PACCMAN implementation, maneuvers are waived if the computed magnitude is less than 3 cm/s and modeled errors are tabulated in Table 2.

Standard FMC

Standard FMC station-keeping results for 100 Monte Carlo simulations, each of 840 revolutions in the 9:2 NRHO, are plotted in Figure 7. Notably different patterns are observed as compared to the PACCMAN implementation. Comparing Figure 7(a) to Figure 4(a) and Figure 7(b) to Figure 4(b), it is apparent that perilune position and phase errors may be significantly higher using the Standard FMC strategy. Indeed Figure 7(b) suggests that Standard FMC does not effectively secure a spacecraft in the appropriate phase with the reference orbit. A comparison of the results in Figure 7(c) and 4(c) indicates that the Standard FMC strategy generally requires lower cumulative maneuver costs over the simulation duration. However, the Standard FMC strategy may not be stable; several Monte Carlo trials reflect sharp increases in cumulative ΔV, perilune position, and perilune phase error near the end of the trial.

The maneuver patterns implemented using Standard FMC, and plotted in Figure 7(d), are also significantly different from those obtained from a PACCMAN strategy. While PACCMAN maneuvers occur in a characteristic plane (Figure 4(d)), a Standard FMC approach results in maneuvers that occur along a characteristic line. This difference is understood in terms of the number of free

variables and constraints in each strategy. Both strategies possess three control variables (the components of the implemented $\Delta \boldsymbol{V}$), but Standard FMC seeks to satisfy only one constraint (eliminate the state component associated with $\boldsymbol{f}_1(t_0)$) whereas PACCMAN is formulated to satisfy two ($\dot{x}$ at perilune and time of perilune arrival). Both strategies ultimately solve a linear system of equations, either once in the case of Standard FMC or iteratively in the PACCMAN algorithm. When solved with a minimum ΔV update, a unique optimal direction emerges from Standard FMC, whereas an optimal plane is identified from a PACCMAN implementation. Notably, the results illustrated in Figure 7 are similar to targeting $\dot{x}$ at perilune only, as considered by Davis et al.[16]

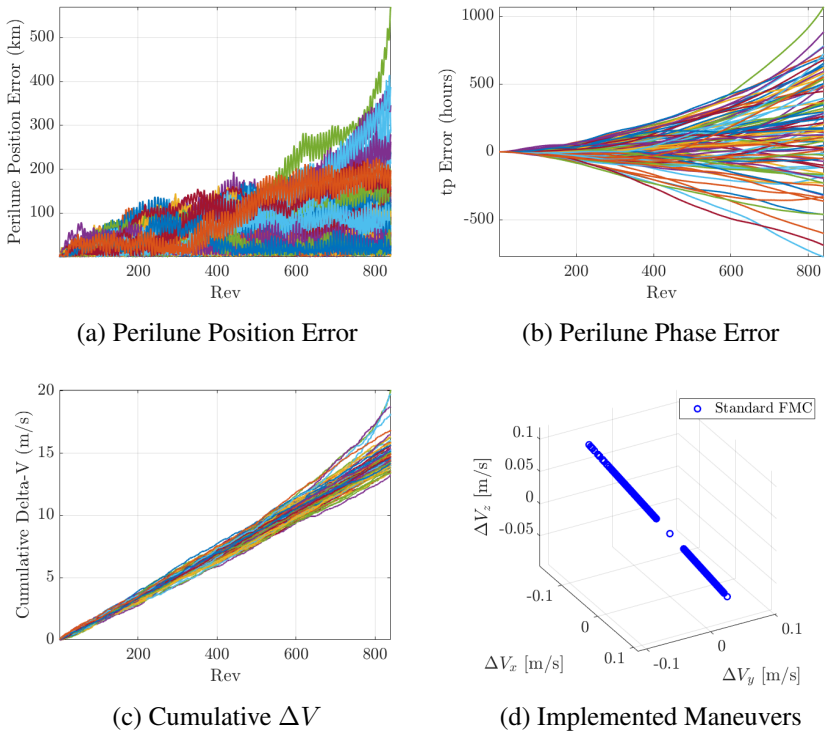

(a) Perilune Position Error

(b) Perilune Phase Error

(c) Cumulative ΔV

(d) Implemented Maneuvers

Figure 7: Standard FMC Monte Carlo Results

Even though PACCMAN and Standard FMC exhibit significant differences in terms of station-keeping performance and maneuver directions, the underlying dynamics leveraged by each strategy are similar. In Figure 8, pre-maneuver and post-maneuver distributions for state components corresponding to exponential growth and decay in the variational state are plotted, as well as distributions for the linear growth term. Comparing Figure 8(a) to Figure 5(a) and Figure 8(b) to 5(b), both strategies apparently reduce the unstable component of a spacecraft variational state while also increasing the stable component. Indeed, Standard FMC is designed to completely remove the unstable component; the width of the distribution in Figure 8(a) is due to waived maneuvers that result in no component change. It is noted that the apparent truncation of the post-maneuver distribution in Figure 8(b) is an artifact of plotting both histograms using the same bins. This approach is needed to clearly observe the differences in the distributions. Figure 8(c) illustrates that Standard FMC enacts almost no change in the component of the spacecraft state associated with linear growth. This observation, along with a comparison to the PACCMAN results in Figure 6, suggests some control

over this state component may be necessary to effectively secure the phase in the 9:2 NRHO and inspires the consideration of a modified FMC strategy.

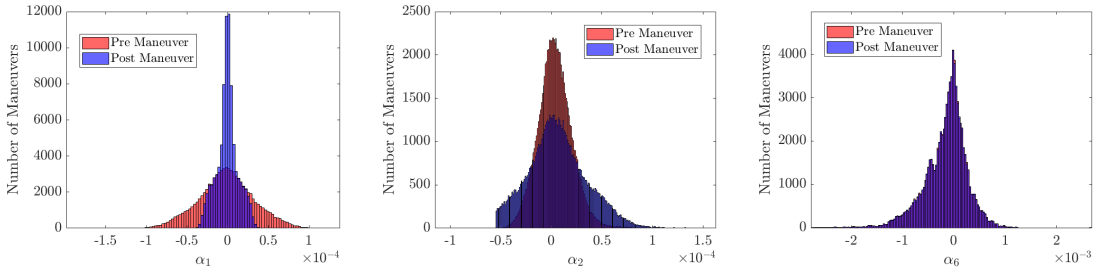

(a) Unstable Component (α_1) (b) Stable Component (α_2) (c) Linear Growth (α_6)

Figure 8: Standard FMC Floquet Components

Modified FMC

The inability of the Standard FMC strategy to secure the spacecraft phase in the 9:2 NRHO suggests that eliminating only the unstable component of the variational state is insufficient for this particular orbit. One possible modification to improve performance is to also eliminate the component of the spacecraft variational state associated with linear growth. This Modified FMC strategy is implemented by constructing a solution to Equation (35) with the objective function in Equation (36) such that large nonzero weights are placed on state components corresponding to exponential and linear growth (α_1 and α_6). To minimize ΔV, nonzero weights are also incorporated on the maneuver components. In this investigation, W_{flo} and $\boldsymbol{b}$ are selected such that

$$W_{flo} = \text{diag}(\begin{bmatrix}1000000 & 0 & 0 & 0 & 0 & 1000000 & 1 & 1 & 1\end{bmatrix}) \qquad \boldsymbol{b} = 0_{9\times 1}.$$

Monte Carlo results for 100 trials, each for 840 revolutions in the 9:2 NRHO, using the Modified FMC strategy are plotted in Figure 9.

The results of a Modified FMC implementation have more similarity to PACCMAN than the Standard FMC approach. A comparison of Figures 4(a) and 9(a) suggests comparable perilune position error between the PACCMAN and Modified FMC strategies. Inspection of Figure 9(b) and 7(b) reveals that the Modified FMC strategy is more effective for maintaining the spacecraft phase in the NRHO than Standard FMC. However, secular growth in the phase error is still observed for the Modified FMC strategy, that is not present in the PACCMAN results in Figure 4(b). Comparing Figures 4(c) and 9(c), it is observed that the Modified FMC strategy is generally more expensive in terms of maneuver costs than PACCMAN. Similar to the PACCMAN implementation, the Modified FMC approach results in a characteristic maneuver plane, as seen in Figure 9(d). This plane is, in fact, identical to the optimal maneuver plane in which PACCMAN maneuvers are executed, as illustrated in Figure 10. It is also notable that the "stripes" associated with the PACCMAN strategy observed in Figure 10 are approximately parallel to the line defined by the Standard FMC maneuvers. This pattern is an artifact of targeting $\dot{x}$ only to initialize the targeting of $\dot{x}$ and t_p together in the PACCMAN scheme. Introducing the t_p target essentially results in stepping the targeted solution off of an optimal direction to satisfy the additional constraint.

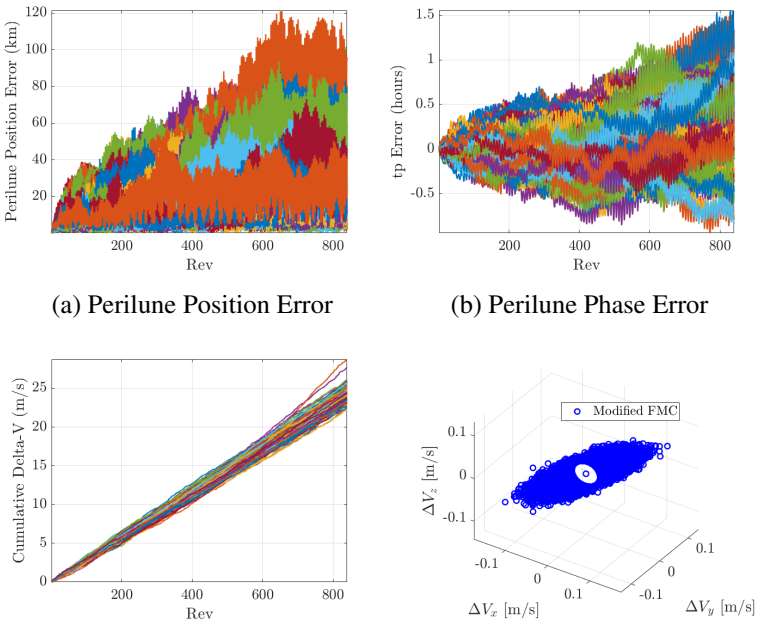

(a) Perilune Position Error (b) Perilune Phase Error

(c) Cumulative ΔV (d) Implemented Maneuvers

Figure 9: Modified FMC Monte Carlo Results

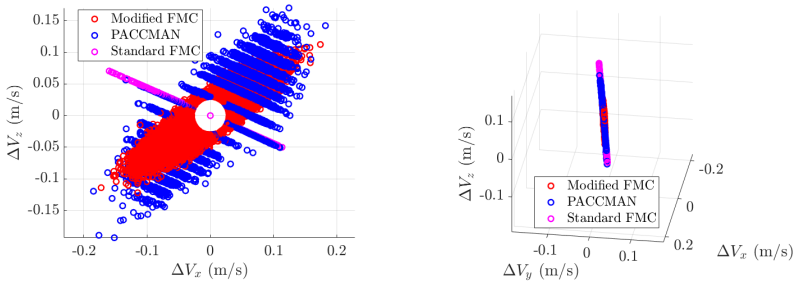

(a) (b)

Figure 10: PACCMAN and FMC Implemented Maneuver Overlay

It is also useful to observe pre-maneuver and post-maneuver distributions of spacecraft variational state components using the Modified FMC strategy, as expressed in terms of the Floquet modes. The distributions of state components corresponding to growth or decay with time are plotted in Figure 11. Similar to the Standard FMC strategy, as well as PACCMAN, Modified FMC results in a significant decrease in the unstable variational state component, while also increasing the stable state component. As designed, the modification of the weighting matrix in solving the FMC problem results in a decreased component of the spacecraft variational state along the generalized eigenvector direction associated with a linear change (Figure 11(c)). Once again, the presence of nonzero α_1 and α_6 coefficients in the post maneuver distributions plotted in Figures 11(a) and 11(c) is due to waived maneuvers that enact no change on the respective state components. Recall that a *small* contraction is observed for the α_6 distribution in the PACCMAN strategy, as seen in Figure 6. Comparing

Figures 6 and 11(c), it is clear that the Modified FMC strategy tends to enact more control over this state component than PACCMAN.

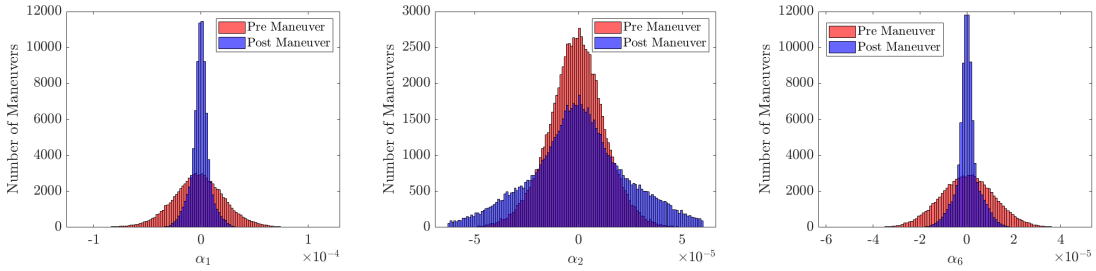

(a) Unstable Component (α_1) (b) Stable Component (α_2) (c) Linear Growth (α_6)

Figure 11: Modified FMC Floquet Components

Additional insight is offered by comparing plots of the perilune phase error for the Modified FMC and PACCMAN strategies during a single Monte Carlo trial. A representative plot appears in Figure 12. The Modified FMC strategy during the trial in Figure 12 tends to produce high frequency oscillatory behavior associated with the perilune phase error and, while effective for preventing the large phase error growth seen in Figure 7(b), does not appear to fully stabilize the spacecraft phase in the NRHO as accomplished in the PACCMAN strategy. This difference in behavior and high frequency oscillation in phase suggests that the total elimination of the α_6 component does not occur in the PACCMAN strategy. It is possible that additional adjustment of the weighting matrix W_{flo} and the target vector $\boldsymbol{b}$ could improve the effectiveness of the Modified FMC strategy and increase parity with the PACCMAN scheme. Constructing the Floquet mode vectors from an isochronous correspondence with the reference orbit, as opposed to a fixed true anomaly, is also an option. These modifications are areas of continued investigation and highlight the flexibility of a Modified FMC strategy as outlined by Equations (35) and (36); such changes are easy to implement via suitable alteration of the weighting matrix and target vector.

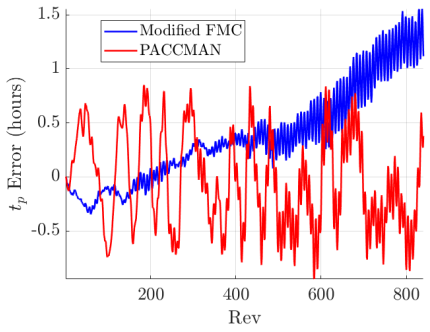

Figure 12: Representative Phase Error Plots

PRINCIPAL STRETCHING DIRECTION CONTROL RESULTS

To implement the Principal Stretching Direction Control strategy, an appropriate time horizon over which to compute the state transition matrix associated with the reference orbit is required. Recall that the PSDC strategy produces a maneuver that is predicted to reduce the magnitude of

a spacecraft variational state relative to some reference trajectory over the specified time horizon. Since maneuvers are allowed once per revolution along the reference orbit, the horizon time is selected as the period of the orbit. The reference state from which the STM is generated reflects an isochronous correspondence along the reference NRHO, due to the dependence of the STM on time. Maneuvers are implemented at an osculating true anomaly value equal to 200° and waived if the maneuver magnitude is less than 3 cm/s. Orbit maintenance error modeling is consistent with the other stationkeeping strategies considered previously. Results for 100 Monte Carlo trials of 840 revolutions are plotted in Figure 13.

The PSDC strategy is extremely effective for maintaining a spacecraft close to the reference periodic orbit. The results plotted in Figures 13(a) and 13(b) demonstrate that PSDC bounds the perilune position and arrival time error by 5 km and 5 minutes over the duration of the simulation. These errors are significantly smaller than those produced using the PACCMAN approach, or any of the FMC methods to be evaluated. Fluctuations in the perilune position and arrival time for the PSDC scheme also display no secular growth, suggesting the algorithm is stable. The improved error levels do exhibit increased station-keeping costs, as is obvious by comparing Figure 13(c) to Figures 4(c), 7(c), and 9(c). In fact, the average total station-keeping cost using PSDC is approximately twice that observed for the PACCMAN and Modified FMC strategies. In contrast to the other approaches examined in this investigation, no characteristic maneuver direction or plane emerges for the PSDC implementation. It is noted that in this particular orbit, PSDC solves a square system. Hence, no minimum ΔV solution, among a range of possibilities, is determined since the problem is fully constrained. Comparing the Monte Carlo results plotted in Figures 4, 7, 9, and 13, the PSDC strategy results in smaller perilune errors for the 9:2 NRHO but results in higher average stationkeeping costs as compared to the other strategies. It is possible that adjusting the scalar weight C_t and tolerances in the PACCMAN scheme could reduce the errors observed for that strategy; only one set of nominal parameters corresponding to Gateway is considered in this investigation. Similarly, adjustment of the weighting matrix W_{flo} and target vector $\boldsymbol{b}$ in the Modified FMC approach could reduce the observed errors for that strategy. One advantage of the PSDC scheme, as compared to the FMC strategies, is that the reference trajectory need not be periodic.

Principal Stretching Direction Control yields notably different station-keeping performance from the other strategies, but similarities do exist in terms of the invariant dynamical structures leveraged by the various methods. From Figures 14(a) and 14(b), the PSDC scheme results in a reduction in the unstable component of a spacecraft's variational state, while also increasing the stable component, similar to both the PACCMAN and FMC strategies. Figure 14(c) demonstrates that, consistent with the PACCMAN and Modified FMC strategies, PSDC maneuvers reduce the state component associated with linear growth as well. The distributions in Figures 6 and 14(c) suggest that some control over the component of a spacecraft variational state corresponding to the linear growth direction may be necessary for the 9:2 NRHO.

CONCLUDING REMARKS

In this investigation, several available orbit maintenance strategies for halo orbits are compared within the context of the CR3BP 9:2 synodic resonant NRHO. Velocity constrained crossing control and Floquet Mode Control are existing strategies that have been examined for station-keeping in halo orbits by other authors. Modifications to the conventional Floquet Mode Control strategy are introduced in this investigation to aid in phase preservation within the selected reference orbit. Floquet theory is also employed to explore the underlying dynamics leveraged by each of the strate-

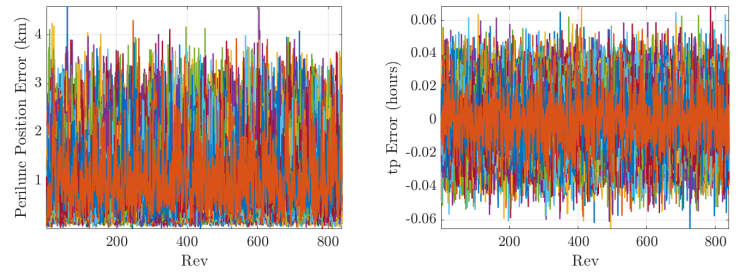

(a) Perilune Position Error (b) Perilune Phase Error

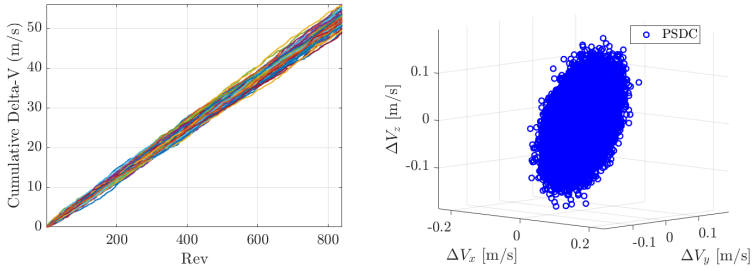

(c) Cumulative ΔV (d) Implemented Maneuvers

Figure 13: PSDC Monte Carlo Results

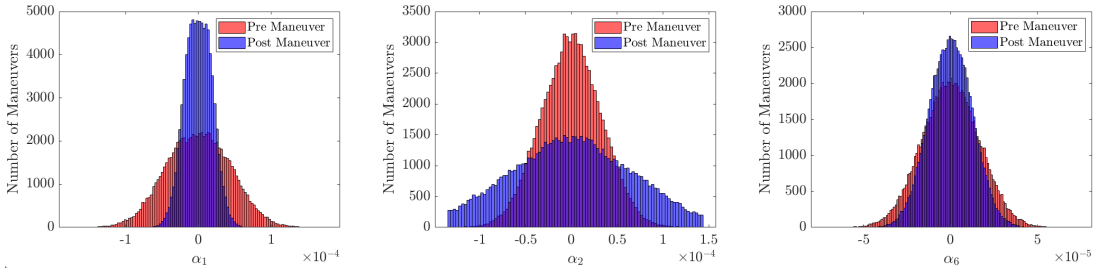

(a) Unstable Component (α_1) (b) Stable Component (α_2) (c) Linear Growth (α_6)

Figure 14: PSDC Floquet Components

gies. All approaches effectively remove the unstable component of a spacecraft variational state while also increasing the magnitude of the stable component. For effective phase maintenance, perhaps desirable for eclipse avoidance in applications, the component of a spacecraft variational state associated with linear growth is also controlled. This direction associated with linear growth corresponds to a generalized eigenvector from the monodromy matrix associated with the underlying periodic orbit and results from the presence of an integral of motion in the CR3BP.

Information available from the Cauchy Green Strain Tensor is incorporated into an additional station-keeping scheme, termed Principal Stretching Direction Control. Inspired by Floquet Mode Control, this strategy uses the eigenvector directions of the CGT to compute a maneuver that is predicted to decrease the magnitude of a spacecraft variatonal state relative to a reference trajectory over a specified time horizon. Notably, this strategy does not require a reference trajectory to be

periodic, nor does it require the selection of any state components for targeting *a priori*. However, an appropriate time horizon must be selected. The PSDC approach offers the benefit of maintaining a spacecraft more closely to the reference 9:2 NRHO than the other strategies, but annual station-keeping costs are significantly higher. It is emphasized that adjustment of weights and tolerances in the PACCMAN and FMC approaches could potentially reduce the observed errors for these strategies. In applications where a reference periodic orbit or trajectory must be precisely followed, PSDC appears to be a useful strategy.

ACKNOWLEDGEMENTS

The authors would like to thank the School of Aeronautics and Astronautics at Purdue University, as well as the Rune and Barbara Eliason Visualization Laboratory, for financial support and facilities. Portions of this work were completed in collaboration with NASA Johnson Space Center and at Purdue University under Grant NASA JSC 80NSSC18M0122. The authors would also like to especially thank Stephen Scheuerle, Brian McCarthy, Emily Zimovan-Spreen, and the fellow members of the Purdue Multi-Body Dynamics Research Group for helpful suggestions and discussions.

REFERENCES

[1] E. Zimovan, K. Howell, and D. Davis, "Near rectilinear halo orbits and nearby higher-period dynamical structures: orbital stability and resonance properties," *Celestial Mechanics and Dynamical Astronomy*, Vol. 132, June 2020.

[2] D. E. Lee, "Gateway Destination Orbit Model: A Continuous 15 Year NRHO Reference Trajectory," Aug. 2019. NTRS Author Affiliations: NASA Johnson Space Center NTRS Report/Patent Number: JSC-E-DAA-TN72594 NTRS Document ID: 20190030294 NTRS Research Center: Johnson Space Center (JSC).

[3] B. Cheetham, "Cislunar Autonomous Positioning System Technology Operations and Navigation Experiment (CAPSTONE)," *ASCEND 2020*, Virtual Event, American Institute of Aeronautics and Astronautics, Nov. 2020.

[4] D. Folta, T. Pavlak, K. Howell, M. Woodard, and D. Woodfork, "Stationkeeping of Lissajous Trajectories in the Earth-Moon System with Applications to ARTEMIS," *Advances in the Astronautical Sciences*, Vol. 136, Jan. 2010.

[5] D. C. Folta, T. A. Pavlak, A. F. Haapala, K. C. Howell, and M. A. Woodard, "Earth–Moon libration point orbit stationkeeping: Theory, modeling, and operations," *Acta Astronautica*, Vol. 94, Jan. 2014, pp. 421–433.

[6] D. C. Davis, S. T. Scheuerle, D. A. Williams, F. S. Miguel, E. M. Zimovan-Spreen, and K. C. Howell, "Orbit Maintenance Burn Details for Spacecraft in a Near Rectilinear Halo Orbit," *AAS/AIAA Astrodynamics Specialist Conference*, Charlotte, North Carolina, 2022.

[7] C. Simo, G. Gomez, J. Llibre, and R. Martinez, "Stationkeeping of a quasiperiodic halo orbit using invariant manifolds," Vol. 255, Nov. 1986, pp. 65–70.

[8] K. Howell and T. Keeter, "Station-Keeping Strategies for Libration Point Orbits: Targer Point and Floquet Mode Approaches," *AAS/AIAA Spaceflight Mechanics Meeting*, Albuquerque, New Mexico, Feb. 1995.

[9] G. Gomez, K. Howell, J. Masdemont, and C. Simo, "Station-Keeping Strategies For Translunar Libration Point Orbits," *Advances in the Astronautical Sciences*, Vol. 99, Jan. 1998.

[10] A. Farrés, C. Gao, J. J. Masdemont, G. Gómez, D. C. Folta, and C. Webster, "Geometrical Analysis of Station-Keeping Strategies About Libration Point Orbits," *Journal of Guidance, Control, and Dynamics*, Vol. 45, June 2022, pp. 1108–1125.

[11] D. Guzzetti, E. Zimovan, K. Howell, and D. Davis, "Stationkeeping Analysis for Spacecraft in Lunar Near Rectilinear Halo Orbits," *AAS/AIAA Space Flight Mechanics Meeting*, San Antonio, Texas, Feb. 2017.

[12] V. Muralidharan and K. C. Howell, "Leveraging stretching directions for stationkeeping in Earth-Moon halo orbits," *Advances in Space Research*, Vol. 69, Jan. 2022, pp. 620–646.

[13] W. E. Wiesel and D. J. Pohlen, "Canonical Floquet theory," *Celestial Mechanics and Dynamical Astronomy*, Vol. 58, Jan. 1994, pp. 81–96.

[14] V. Muralidharan, *Stretching Directions in Cislunar Space: Stationkeeping and an Application to Transfer Trajectory Design*. PhD Dissertation, Purdue University, West Lafayette, IN, 2021.

[15] C. Simó, G. Gómez, J. Llibre, R. Martínez, and J. Rodríguez, "On the optimal station keeping control of halo orbits," *Acta Astronautica*, Vol. 15, June 1987, pp. 391–397.

[16] D. C. Davis, F. S. Khoury, K. Howell, and D. Sweeney, "Phase Control and Eclipse Avoidance in Near Rectilinear Halo Orbits," *AAS Guidance Navigation and Control Conference*, Breckenridge, Colorado, 2020.